Crack-damage quantification based on stochastic optimization of finite element models with data-driven features

Enora Denimal, Szymon Gres

Crack-damage quantification based on stochastic optimization of finite element models with data-driven features

E. Denimal [1] **, S. Greś** [2]

[1] Univ. Gustave Eiffel, Inria, COSYS-SII, I4S
Campus de Beaulieu, 35042 Rennes, France
e-mail: **enora.denimal@inria.fr**

[2] Aarhus University, Department of Civil and Architectural Engineering
Nordre Ringgade 1, 8000 Aarhus, Denmark

Abstract

The vibration-based Structural Health Monitoring plays a central role in ensuring the safe operation of infrastructures by monitoring their structural integrity based on data collected by sensors. While damage detection has reached maturity, the localization and the quantification of small-scale damage remain an open challenge. To address it, both the localization and the quantification of damage are often posed as an updating problem of a Finite Element Model (FEM) of the operating structure, minimizing the misfit between some features computed from response measurements of a faulty structure and its FEM in a reference, healthy condition. This paper investigates the choice of the features for the design of the objective function to quantify structural cracks. For this purpose, a FEM of a beam with a transverse crack is developed and parametrized by the second moment of area of the elements to locate and quantify the crack-related damage. Subsequently, the impact on the choice of the objective function is discussed based on a small-samples Monte Carlo study.

1 Introduction

Three pillars of Structural Health Monitoring (SHM) are fault detection (is the structure changed?), localization (where?) and quantification (how big is the change?) [1]. Whereas the detection of damage from vibration measurements is well established, e.g., in [2–6], the localization and quantification of damage is more complex, and requires additional physical information on the examined structure [7–10]. In this respect, few complete frameworks for damage identification exist, e.g., [11–15]. Some methods are constrained to a specific structural models, e.g., beams [12], tailored to a specific damage type, e.g., crack damage [13–15], while other methods incorporate a global physical information from a FE model allowing for applications to more general systems. In this context, the sensitivities of damage features computed from the structural responses can be used to infer FE model parameter changes in [11], under the assumption of small damage extents. Contrary to these approaches, FE model optimization-based methods are usually not limited by the structural type or by the damage extent. Therein model updating is a generic term encompassing a family of many methods [16, 17], that are often applied in the damage quantification context [18–21]. Model updating methods, however, are often poorly conditioned due to the possibly large FE parameter space in comparison to relatively few parameters that can be extracted from data, which may potentially detract from the reliability of the damage diagnosis procedure, particularly under the uncertainty errors on the estimated features. Among several methods to account for those uncertainty errors, e.g., with Bayesian strategies [13], the recently proposed statistical model-based optimization approach incorporates the uncertainty on the target features into the objective function that is evaluated in a stochastic optimization strategy for the data-model matching.

This paper investigates the choice of the features for the design of the objective function to quantify structural

cracks. For this purpose, a FE model of a beam with a transverse crack is developed. To locate and quantify the crack-related damage, the model is parametrized by the second moments of area of damaged elements. Subsequently, the impact on the choice of the objective function is discussed based on a small-samples Monte Carlo study.

2 Background

The aim of this paper is to estimate a parameter that characterizes damage in a Finite Element (FE) model of a mechanical system. Let $\theta \in \Theta \subset \mathbb{R}^p$ be the parameter vector that contains damage-sensitive parameters of the structural elements of interest for the considered problem within a bounded parameter space Θ. This parametrization is defined after the specific monitoring problem at hand, such that θ contains parameters of the dynamic system whose sensitivity to damage is non-zero and which fully parametrize the considered damage, e.g., Young's modulus, mass density of elements, crack parameters (width, length), among others. Finding the optimal $\hat{\theta}$ can be formulated as an optimization problem, where an objective function $F(\theta)$ is minimized over some bounded parameter space Θ with the purpose of finding the true value of the parameter θ_*.

Assume that the dynamics of the monitored system can be modelled as linear time-invariant (LTI) with d degrees of freedom (DOF), which are described by the differential equation of motion

$$\mathcal{M}^\theta \ddot{q}(t) + \mathcal{D}^\theta \dot{q}(t) + \mathcal{K}^\theta q(t) = u(t) \tag{1}$$

where t denotes the continuous time, and the matrices $\mathcal{M}^\theta$, $\mathcal{D}^\theta$ and $\mathcal{K}^\theta \in \mathbb{R}^{d \times d}$ denote the mass, damping and stiffness matrices, respectively, which depend on the system parameter θ. Vectors $q(t) \in \mathbb{R}^d$ and $u(t)$ $\in \mathbb{R}^d$ denote the continuous-time displacements and the unknown external forces, respectively. Observed at r sensor positions and sampled at discrete time instants $t = k\tau$ with sampling rate $1/\tau$, system (1) can be transformed into the discrete-time state-space model [22]

$$\begin{cases} x_{k+1}^\theta = A^\theta x_k^\theta + w_k \\ y_k^\theta = C^\theta x_k^\theta + v_k \end{cases} \tag{2}$$

where $x_k^\theta \in \mathbb{R}^n$ are the states, $y_k^\theta \in \mathbb{R}^r$ are the outputs e.g., accelerations, velocities, or displacements, vectors w_k and v_k denote the white process and output noise respectively, $A^\theta \in \mathbb{R}^{n \times n}$, $C^\theta \in \mathbb{R}^{r \times n}$ are the state and observation matrices, and $n = 2d$ is the model order. The process noise v_k is assumed to be a stationary process with zero mean and covariance matrix $Q = \mathrm{E}(v_k v_k^T)$, w_k denotes the zero-mean output noise with covariance matrix $R = \mathrm{E}(w_k w_k^T)$, and the covariance between v_k and w_k is $S = \mathrm{E}(v_k w_k^T)$, where $\mathrm{E}(\cdot)$ denotes the expectation operator.

For simplicity, the $(\cdot)^\theta$ notation is dropped in the remainder of this paragraph. Let $\mathcal{R}_i = \mathrm{E}(y_k y_{k-i}^T) = C A^{i-1} G$ be the theoretical output covariances of the measurements, where $G = \mathrm{E}(x_{k+1} y_k^T) = A \Sigma^s C^T + S$ and $\Sigma^s = \mathrm{E}(x_k x_k^T) = A \Sigma^s A^T + Q$. The collection of $\mathcal{R}_i$ can be stacked to form a block Hankel matrix

$$\mathcal{H} = \begin{bmatrix} \mathcal{R}_1 & \mathcal{R}_2 & \ldots & \mathcal{R}_q \\ \mathcal{R}_2 & \mathcal{R}_3 & \ldots & \mathcal{R}_{q+1} \\ \vdots & \vdots & \ddots & \vdots \\ \mathcal{R}_{p+1} & \mathcal{R}_{p+2} & \ldots & \mathcal{R}_{p+q} \end{bmatrix} \in \mathbb{R}^{(p+1)r \times qr}, \tag{3}$$

where p and q are chosen such that $\min(pr, qr) \geq n$ with often $p + 1 = q$. Matrix $\mathcal{H}$ enjoys the factorization property

$$\mathcal{H} = \mathcal{O}(C, A)\, \mathcal{C}(A, G), \tag{4}$$

where the observability and controllability matrices $\mathcal{O}(C, A)$ and $\mathcal{C}(A, G)$ are defined as

$$\mathcal{O}(C, A) = \begin{bmatrix} C \\ CA \\ \vdots \\ CA^p \end{bmatrix}, \quad \mathcal{C}(A, G) = \begin{bmatrix} G & AG & \cdots & A^{q-1}G \end{bmatrix}. \tag{5}$$

Matrices (A, C) can be easily obtained from $\mathcal{M}, \mathcal{D}, \mathcal{K}$ [22] and G is obtained based on the chosen noise properties after [23]. Consistent estimates $\hat{\mathcal{H}}$ can be obtained from the output covariances of the measurements $\{y_k\}_{k=1,\ldots,N+p+q}$

$$\hat{\mathcal{H}} = \mathcal{Y}^+ \mathcal{Y}^{-T}, \tag{6}$$

where the data Hankel matrices $\mathcal{Y}^+$ and $\mathcal{Y}^-$ contain the future and the past time horizons

$$\mathcal{Y}^+ = \frac{1}{\sqrt{N}} \begin{bmatrix} y_{q+1} & y_{q+2} & \cdots & y_{N+q} \\ y_{q+2} & y_{q+3} & \cdots & y_{N+q+1} \\ \vdots & \vdots & \ddots & \vdots \\ y_{p+q+1} & y_{p+q+2} & \cdots & y_{p+q+N} \end{bmatrix}, \quad \mathcal{Y}^- = \frac{1}{\sqrt{N}} \begin{bmatrix} y_q & y_{q+1} & \cdots & y_{N+q-1} \\ y_{q-1} & y_q & \cdots & y_{N+q-2} \\ \vdots & \vdots & \ddots & \vdots \\ y_1 & y_2 & \cdots & y_N \end{bmatrix}. \tag{7}$$

The estimates of $\mathcal{O}(C, A)$ and $\mathcal{C}(A, G)$ can be obtained from a singular value decomposition (SVD) of $\hat{\mathcal{H}}$ thanks to the factorization property (4). The estimates of the modal parameters of system (1) can be then obtained from the estimate of $\mathcal{O}(C, A)$ with, e.g., subspace identification methods [24].

3   Objective functions and model optimization strategy

An estimate of θ_* is obtained by minimizing an objective function that is designed to represent the discrepancy between the estimate of a feature vector computed from measurement data collected under the unknown, true system parameter θ_*, and its counterpart computed from a parametric model. The solution for θ is obtained as

$$\hat{\theta} = \underset{\theta \in \Theta}{\arg\min} \; F(\theta). \tag{8}$$

A decision whether the current model parametrization θ corresponds to the unknown parameter θ_* needs to take into account the uncertainty of the estimated feature and its sensitivity towards the considered parameterization. To assess this equivalence a residual ζ is defined, whose statistical properties can be evaluated as the number of samples goes to infinity. For this, two hypotheses are defined

$$\begin{aligned} \mathrm{H}_0 &: \theta = \theta_* \; \text{(model matched)}, \\ \mathrm{H}_1 &: \theta \neq \theta_* \; \text{(model mismatched)}. \end{aligned} \tag{9}$$

A classic feature used for the residual evaluation and the design of the objective function $F(\theta)$ (8) is based on the modal parameters of the monitored system and their statistical uncertainties [25]. In this work, three sets of damage sensitive features are evaluated in damage residuals that are used as objective functions in data-model optimization, namely

- subspace-based damage residual from [2],
- Hankel matrix difference residual from [26],
- modal parameter-based residual from [27].

A short description of the aforementioned damage residuals is enclosed below.

3.1 Subspace-based damage residual

Let $\mathcal{O}^\theta_{\text{model}}$ be the parametric model-based observability matrix and let $\hat{\mathcal{H}}^{\theta_*}_{\text{data}}$ be the Hankel matrix obtained from a data set of length N. The subspace damage residual is defined after [2] as

$$\hat{\zeta}^\theta_{\text{S}} \overset{\text{def}}{=} \sqrt{N}\text{vec}((U^\theta_{\text{null}})^T \hat{\mathcal{H}}^{\theta_*}_{\text{data}}), \tag{10}$$

where U^θ_{null} is the left null space of $\mathcal{O}^\theta_{\text{model}}$ defined from the SVD partitioned at order n

$$\mathcal{O}^\theta_{\text{model}} = \begin{bmatrix} U^\theta_{\text{sig}} & U^\theta_{\text{null}} \end{bmatrix} \begin{bmatrix} D^\theta_{\text{sig}} & 0 \\ 0 & D^\theta_{\text{null}} \end{bmatrix} \begin{bmatrix} V^{\theta^T}_{\text{sig}} \\ V^{\theta^T}_{\text{null}} \end{bmatrix}. \tag{11}$$

Matrix $\mathcal{O}^\theta_{\text{model}}$ can be obtained by using the FE model-based (A, C) matrices in (5). The residual $\hat{\zeta}^\theta_{\text{S}}$ (10) is zero iff the parameters θ and θ_* correspond, which is evaluated in a Generalized Likelihood Ratio (GLR) test

$$\text{t}^\theta_{\text{S}} = (\hat{\zeta}^\theta_{\text{S}})^T \widehat{\Sigma}^{-1}_{\text{S}} \widehat{\mathcal{J}}_{\text{S}} \left(\widehat{\mathcal{J}}^T_{\text{S}} \widehat{\Sigma}^{-1}_{\text{S}} \widehat{\mathcal{J}}_{\text{S}} \right)^{-1} \widehat{\mathcal{J}}^T_{\text{S}} \widehat{\Sigma}^{-1}_{\text{S}} \hat{\zeta}^\theta_{\text{S}}, \tag{12}$$

where $\widehat{\mathcal{J}}_{\text{S}}$ is the consistent estimate of the sensitivity of the residual w.r.t. model parameter $\mathcal{J}_{\text{S}} = \partial \zeta^\theta_{\text{S}}/\partial\theta\,(\theta_*)$ and $\widehat{\Sigma}_{\text{H}}$ denotes the consistent estimate of the residual covariance. The test value from (12) can be directly used in the objective function for the model optimization as $F_{\text{S}}(\theta) = \text{t}^\theta_{\text{S}}$. When the model features match the features obtained from data, the GLR test statistics follows a central χ^2 distribution with the degrees of freedom $l = \text{rank}(\mathcal{J}_{\text{S}})$. The quantile q_{χ^2} of the underlying χ^2 distribution, satisfying $\int_0^{q_{\chi^2}} f_{\chi^2}(x)dx = \gamma$, where γ is a desired confidence level, can be used to define an acceptance region

$$\Theta_{\text{S}} = \{\theta : \text{t}^\theta_{\text{S}} \leq q_{\chi^2}\}, \tag{13}$$

which comprises all parameter vectors θ for which U^θ_{null} is the left null space of the estimated reference $\hat{\mathcal{H}}^{\theta_*}_{\text{data}}$. Thus, Θ_{S} comprises the statistically plausible solutions for θ_* with regards to the considered models, which allows to stop the optimization search when $\theta \in \Theta_{\text{S}}$.

3.2 Hankel matrix difference

The Hankel matrix difference damage residual is defined after [26] as

$$\hat{\zeta}^\theta_{\text{H}} \overset{\text{def}}{=} \sqrt{N}\text{vec}(\mathcal{O}^\theta_{\text{model}} \hat{\mathcal{Z}}^\dagger_{\text{model}} \hat{\mathcal{Z}}_{\text{data}} - \hat{\mathcal{H}}^{\theta_*}_{\text{data}}), \tag{14}$$

where $\hat{\mathcal{Z}}_{\text{data}}$ and $\hat{\mathcal{Z}}_{\text{model}}$ are defined from the SVD partitioned at order n

$$\begin{bmatrix} \hat{\mathcal{H}}^{\theta_*}_{\text{data}} & \mathcal{O}^\theta_{\text{model}} \end{bmatrix} = \begin{bmatrix} \hat{U}_{\text{sig}} & \hat{U}_{\text{null}} \end{bmatrix} \begin{bmatrix} \hat{D}_{\text{sig}} & 0 \\ 0 & \hat{D}_{\text{null}} \end{bmatrix} \begin{bmatrix} \hat{V}^T_{\text{sig}} & \hat{V}^T_{\text{sig}} \\ \hat{V}^T_{\text{null}} & \hat{V}^T_{\text{null}} \end{bmatrix}, \tag{15}$$

as $\hat{\mathcal{Z}}_{\text{data}} = \hat{D}_{\text{sig}}\hat{V}^T_{\text{sig}}$, $\hat{\mathcal{Z}}_{\text{model}} = \hat{D}_{\text{sig}}\hat{V}^T_{\text{sig}}$. The residual (14) is zero iff the parameters θ and θ_* correspond, which is also evaluated in a GLR test

$$\text{t}^\theta_{\text{H}} = (\hat{\zeta}^\theta_{\text{H}})^T \widehat{\Sigma}^{-1}_{\text{H}} \widehat{\mathcal{J}}_{\text{H}} \left(\widehat{\mathcal{J}}^T_{\text{H}} \widehat{\Sigma}^{-1}_{\text{H}} \widehat{\mathcal{J}}_{\text{H}} \right)^{-1} \widehat{\mathcal{J}}^T_{\text{H}} \widehat{\Sigma}^{-1}_{\text{H}} \hat{\zeta}^\theta_{\text{H}}, \tag{16}$$

where $\widehat{\mathcal{J}}_{\text{H}}$ is the consistent estimate of the sensitivity of the residual w.r.t. model parameter $\mathcal{J}_{\text{H}} = \partial \zeta^\theta_{\text{H}}/\partial\theta\,(\theta_*)$ and $\widehat{\Sigma}_{\text{H}}$ denotes the consistent estimate of the residual covariance. The GLR test value (16) can be directly used in the objective function for the model optimization as $F_{\text{H}}(\theta) = \text{t}^\theta_{\text{H}}$ and an acceptance region

$$\Theta_{\text{H}} = \{\theta : \text{t}^\theta_{\text{H}} \leq q_{\chi^2}\}, \tag{17}$$

is defined based on the similar principles as for the objective function corresponding to the subspace-based residual.

3.3 Modal parameter and MAC difference

As an alternative to objective functions designed based on data-driven residuals (10) and (14), a classic objective function for model optimization can be expressed by the difference between the estimated and the numerical modal parameters [27]. For this purpose, denote $\Delta_{f_i}^\theta$ as the normalized difference between the estimated natural frequency $\hat{f}_i$ and the natural frequency f_i^θ from the model under parameter θ, with

$$\Delta_{f_i}^\theta = 1 - \frac{f_i^\theta}{\hat{f}_i}. \tag{18}$$

For the comparison of the mode shape estimate $\hat{\varphi}_i$ (computed from measurements under unknown system parameter θ_*) to the numerical counterpart ψ_i^θ from the model, the MAC is used. Let $\Delta_{\mathrm{MAC}_i}^\theta$ be the difference between 1 and the respective MAC, defined as

$$\Delta_{\mathrm{MAC}_i}^\theta = 1 - \mathrm{MAC}(\hat{\varphi}_i, \psi_i^\theta). \tag{19}$$

The objective function $F_\mathrm{M}(\theta)$ indicates the distance between the estimated modal parameters and their model counterparts, and it can be expressed as the sum of the respective differences $\Delta_{f_i}^\theta$ and $\Delta_{\mathrm{MAC}_i}^\theta$ for all considered modes $i = 1, \ldots, m$, as

$$F_\mathrm{M}(\theta) = \sum_{i=1}^m \left| \Delta_{f_i}^\theta \right| + \sum_{i=1}^m \Delta_{\mathrm{MAC}_i}^\theta. \tag{20}$$

The corresponding acceptance region is defined based on the confidence intervals derived for the natural frequency estimates $c_{\hat{f}_i}$ and the MAC between an estimate of a mode shape and a mode shape obtained from an FE model t_{MAC_i}, as

$$\Theta_\mathrm{M} = \{\theta : f_i^\theta \in c_{\hat{f}_i} \text{ and } \mathrm{MAC}(\hat{\varphi}_i, \psi_i^\theta) > t_{\mathrm{MAC}_i} \text{ for all } i = 1, \ldots, m\}. \tag{21}$$

3.4 Model optimization with the modified Covariance Matrix Adaptation Evolution Strategy (CMA-ES)

Starting with the initial value $\theta = \theta_\mathrm{init}$ corresponding to the model in the reference state, the CMA algorithm consists in generating λ model candidates θ_j^g, $j = 1, \ldots, \lambda$, in each population g, by sampling a multivariate Gaussian distribution. The sampling is carried out on the considered parameter subset for the subsequent population $g + 1$ as

$$(\theta_j)^{g+1} = m^g + \varepsilon_j, \quad \varepsilon_j \sim \sigma^g \mathcal{N}(0, C^g), \tag{22}$$

where $j = 1, \ldots, \lambda$ and m^g is a weighted mean of the model candidates $(\theta_j)^g$ in the parent generation. The covariance matrix C^g of the added Gaussian noise ε_j represents the amplitude of sampling, and the scaling factor σ^g determines the range of the search. For the convergence to a solution, the stopping criteria (13), (17) and (21) are included in the optimization of the objective functions $F_\mathrm{S}(\theta)$, $F_\mathrm{H}(\theta)$ and $F_\mathrm{M}(\theta)$, which ceases when the respective acceptance regions are reached. Then the final solution is computed as the mean of the selected t model candidates $\theta_{j_k}^g \in \overline{\Theta}$ in the last population g that are lying in the acceptance region, with

$$\theta_\mathrm{sol} = \tfrac{1}{t} \sum_{k=1}^t \theta_{j_k}^g. \tag{23}$$

4 Numerical case study

The mechanical system under study consists of a circular beam of radius R and length L. The beam is simply supported at both ends and the values of the model parameters are given in Table 1. The damage is emulated as a transverse crack located at $L/3$ based on [28]. The beam is discretized with 30 Euler beam elements, where each node has four degrees of freedom (dof). The damping matrix is taken as a Rayleigh damping, i.e., $\mathcal{D} = \alpha\mathcal{M} + \beta\mathcal{K}$ with $\alpha = 0.66$ and $\beta = 1.2^{-6}$. The model is illustrated in Figure 1.
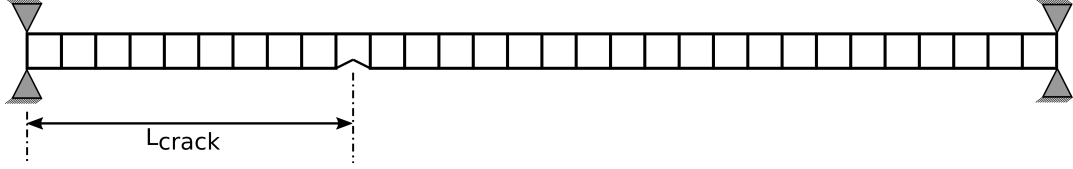

Figure 1: The considered parametrized beam finite element model.

Table 1: Mechanical and geometrical properties of the cracked beam

Parameter	Value
Length (m)	1
Radius (m)	0.05
Young's modulus (Pa)	2×10^{11}
Shear modulus (Pa)	7.1×10^{10}
Density (kg/m^3)	7800
Poisson ratio	0.3

The crack model is based on the model of Mayes and Davies [29], where it has been proposed to recreate the local flexibility induced by the crack as a change in the second moment of area. In what follows, the second moment of area at the location of the crack is reduced by ΔI

$$\Delta I = I_0 \left(\frac{R/l(1 - \nu^2)F(\mu)}{1 + (R/l)(1 - \nu^2)F(\mu)} \right), \tag{24}$$

where I_0 is the second moment of area of the uncracked section, R is the beam radius, ν is the Poisson's ratio, l is the element length, $\mu = h/R$ is the non-dimensional crack depth and h is the depth of the crack. $F(\mu)$ is the compliance function depending on the non-dimensional crack-depth detailed in [29]. Subsequently, the stiffness matrix $\mathcal{K}^i_{\text{crack}}$ of the cracked element i is defined as

$$\mathcal{K}^i_{\text{crack}} = \frac{E}{l^3} \begin{bmatrix} 12I_X & 0 & 0 & 6lI_X & -12I_X & 0 & 0 & 6lI_X \\ & 12I_Y & -6lI_Y & 0 & 0 & -12I_Y & -6lI_Y & 0 \\ & & 4l^2I_Y & 0 & 0 & 6lI_Y & 2l^2I_Y & 0 \\ & & & 4l^2I_X & -6lI_X & 0 & 0 & 2l^2I_X \\ & & & & 12I_X & 0 & 0 & -6lI_X \\ & & Sym. & & & 12I_Y & 6lI_Y & 0 \\ & & & & & & 4l^2I_Y & 0 \\ & & & & & & & 4l^2I_X \end{bmatrix}, \tag{25}$$

where I_X and I_Y are the new moment of inertia [28]. The global stiffness matrix $\mathcal{K}_{\text{crack}}$ is defined as the concatenation on the diagonal of the cracked matrix of each element

$$\text{diag}(\mathcal{K}_{\text{crack}}) = (0_{8\times8} \quad \cdots \quad 0_{8\times8} \quad \mathcal{K}^i_{\text{crack}} \quad 0_{8\times8} \quad \cdots \quad 0_{8\times8}). \tag{26}$$

Note that $\mathcal{K}^i_{\text{crack}} = 0_{8\times8}$ when there is no crack. Finally, the structural matrices of the cracked beam are written as $\mathcal{M}_c = \mathcal{M}$, $\mathcal{K}_c = \mathcal{K} - \mathcal{K}_{\text{crack}}$ and $\mathcal{D}_c = \alpha\mathcal{M}_c + \beta\mathcal{K}_c$, where the subscript c denotes the cracked
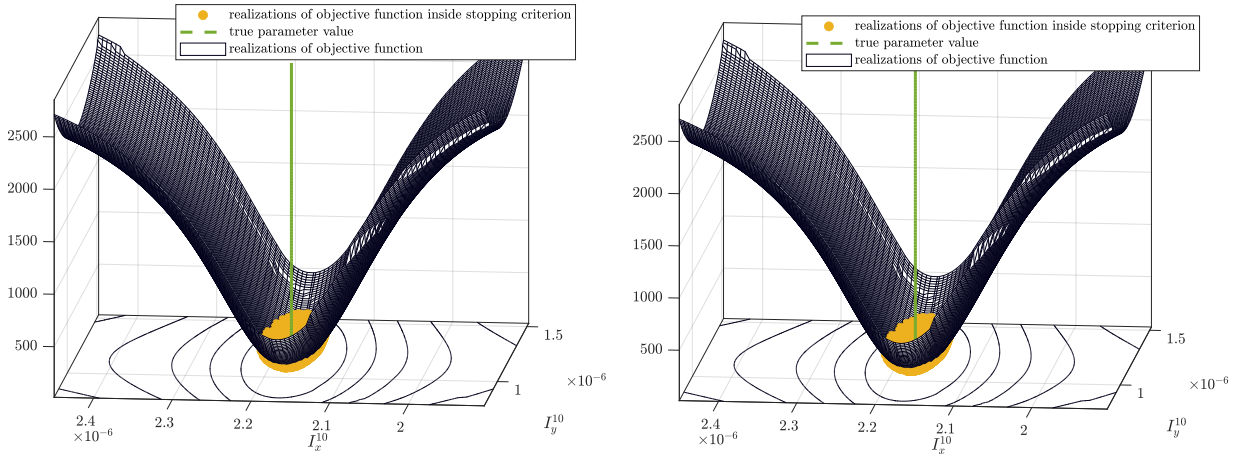
Figure 2: Objective function $F_{\mathrm{S}}(\theta)$ (left) and $F_{\mathrm{H}}(\theta)$ (right) for the parameter pair (I_x^{10}, I_y^{10}).
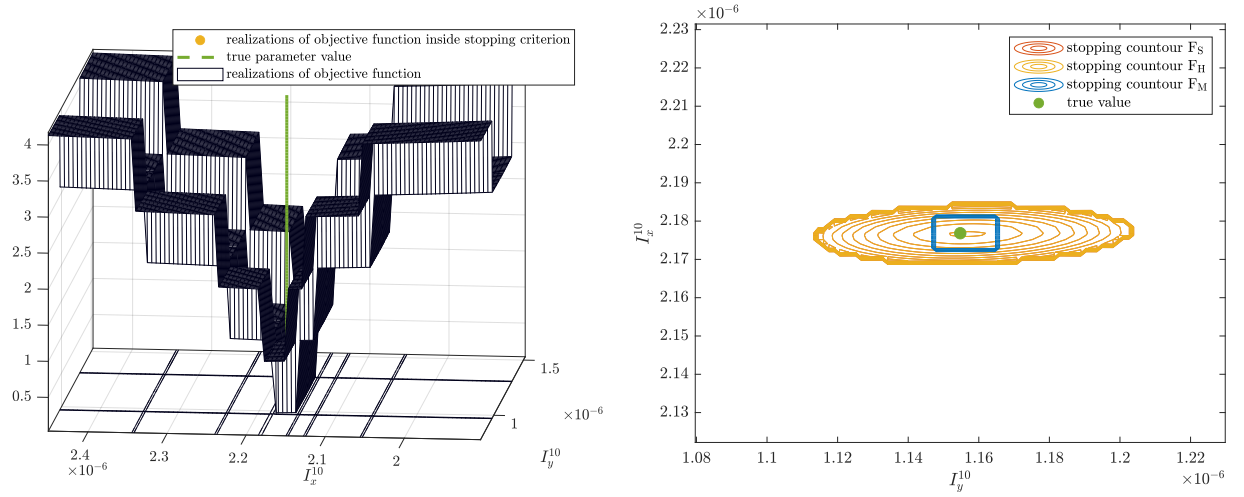

Figure 3: Objective function $F_{\mathrm{M}}(\theta)$ (left) for the parameter pair (I_x^{10}, I_y^{10}). Contour of parameter sets satisfying the stopping criteria (right).

system.

In the following study, the crack is modelled in the 10th element and the non-dimensional crack depth is $\mu = 0.8$. The beam is excited with a white noise at all dofs in x and y directions. Three biaxial sensors located at 5, 20 and 25 dof in x and y directions are considered. As the presence of the crack reduces the second moments of area of the beam section, the model is parametrized by these second moments of area. As such, there are 2 parameters for each element, where I_x^i and I_y^i will denote the second moment of area in the x and y direction of the element i, respectively.

4.1 Preliminary analysis

Before the model optimization, the considered objective functions and the corresponding acceptance regions are examined. Functions $F_{\mathrm{H}}(\theta)$, $F_{\mathrm{M}}(\theta)$ and $F_{\mathrm{S}}(\theta)$ map the p-dimensional parameter space to a multidimensional plane whose shape can easily be illustrated for $p = 2$, i.e., in two dimensional parameter space. For this purpose, let $\theta \in \Theta^2$ contains the second moments of area in x and y directions for the damaged element, i.e., element number 10. The objective functions $F_{\mathrm{H}}(\theta)$, $F_{\mathrm{S}}(\theta)$ and $F_{\mathrm{M}}(\theta)$ are then obtained for a parameter pair $I_x^{10} \in [7.79 \cdot 10^{-7}, 1.53 \cdot 10^{-6}]$, $I_y^{10} \in [1.90 \cdot 10^{-6}, 2.45 \cdot 10^{-6}]$ and are displayed in Figure 2 and in the left part of Figure 3. Note that the remaining second moments of area are considered to correspond to an undamaged model. Contours of parameters that satisfy the stopping criteria are shown in the right part of
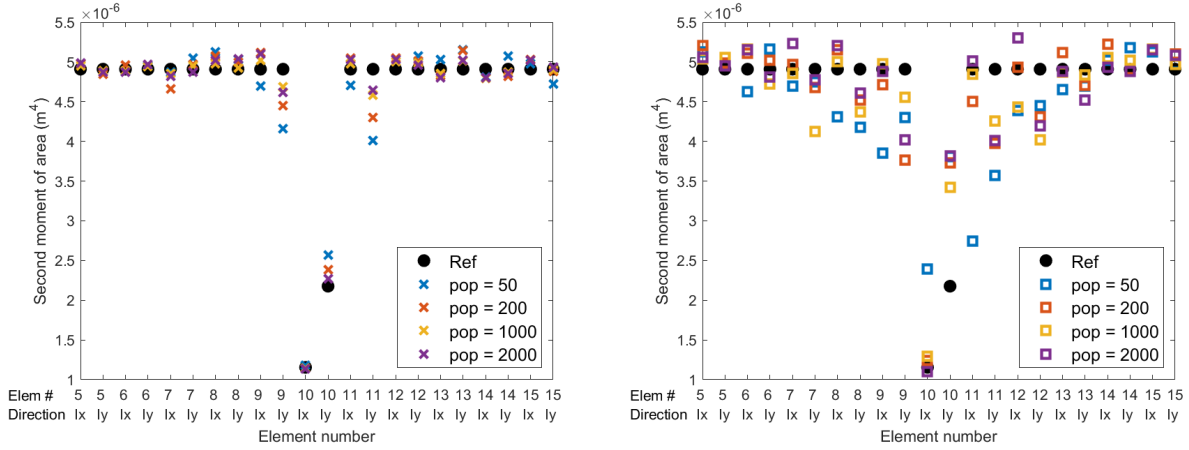
Figure 4: Average second moments of area for elements 5 to 15 in x and y direction. $F_\mathrm{M}(\theta)$ objective function (left). $F_\mathrm{S}(\theta)$ objective function (right)

Table 2: CMA-ES population size, the associated number of evaluations and the simulation time for $F_\mathrm{M}(\theta)$ and $F_\mathrm{S}(\theta)$.

Case id.	Population size	No. evaluations		Simulation time	
		$F_\mathrm{M}(\theta)$	$F_\mathrm{S}(\theta)$	$F_\mathrm{M}(\theta)$	$F_\mathrm{S}(\theta)$
1	50	8000	2200	1 min	1.1 h
2	200	24600	7200	2.7 min	3 h
3	1000	76000	23000	8 min	9 h
4	2000	114000	35000	13 min	15.5 h

Figure 3.

It can be viewed that each objective function is convex in the considered parameter space and for each function the true value of the parameter lies in the respective acceptance region. The shape of the objective functions $F_\mathrm{S}(\theta)$ and $F_\mathrm{H}(\theta)$, and the respective contours of parameters laying in the acceptance region is identical. The $F_\mathrm{M}(\theta)$ is stepper and more rugged than $F_\mathrm{S}(\theta)$ and $F_\mathrm{H}(\theta)$, and the corresponding acceptance region is narrower. Based on this, it is expected that the optimization of $F_\mathrm{M}(\theta)$ will yield more precise estimates of θ_*. Moreover, for all the considered objective functions, the acceptance region for I_x is narrower than for I_y, thus it is expected that the estimates of I_x will be more precise than the estimates of I_y.

Next, the impact of the population size of the CMA-ES is examined. As $F_\mathrm{S}(\theta)$ and $F_\mathrm{H}(\theta)$ turn out to be numerically identical, only $F_\mathrm{S}(\theta)$ and $F_\mathrm{M}(\theta)$ are considered. The model optimization is performed on the second moment of area in x and y directions for elements 5 to 15. Four population sizes are considered, i.e., $[50, 200, 1000, 2000]$. For each population size, 20 evaluations of the respective objective functions are conducted. The average values of the solution from each function is displayed in Figure 4, where it is confronted to the reference values of the second moments of area of the cracked beam (black dots). The number of evaluations and the total simulation time of the optimization are summarized in Table 2.

It can be viewed that the average optimization results obtained with $F_\mathrm{M}(\theta)$ correspond well to the true value of the second moment of area of the cracked beam. For population sizes below 200, a drop in the second moment of area at elements around element 10 is observed, which is more significant for the second moment of area in y direction. The average optimization results obtained for $F_\mathrm{S}(\theta)$ are less precise than for $F_\mathrm{M}(\theta)$. A drop in the second moments of area is observed between elements 8 and 12 for all the considered cases and is more significant for a small population sizes than for larger populations. The lower precision of $F_\mathrm{S}(\theta)$, and consequently $F_\mathrm{H}(\theta)$, than $F_\mathrm{M}(\theta)$ is expected due to larger acceptance region, see the right part of Figure 3. The optimization performance with the modal parameter-based objective function is also superior than the optimization with the subspace-based data-driven metrics, see Table 2. While the optimization with $F_\mathrm{M}(\theta)$
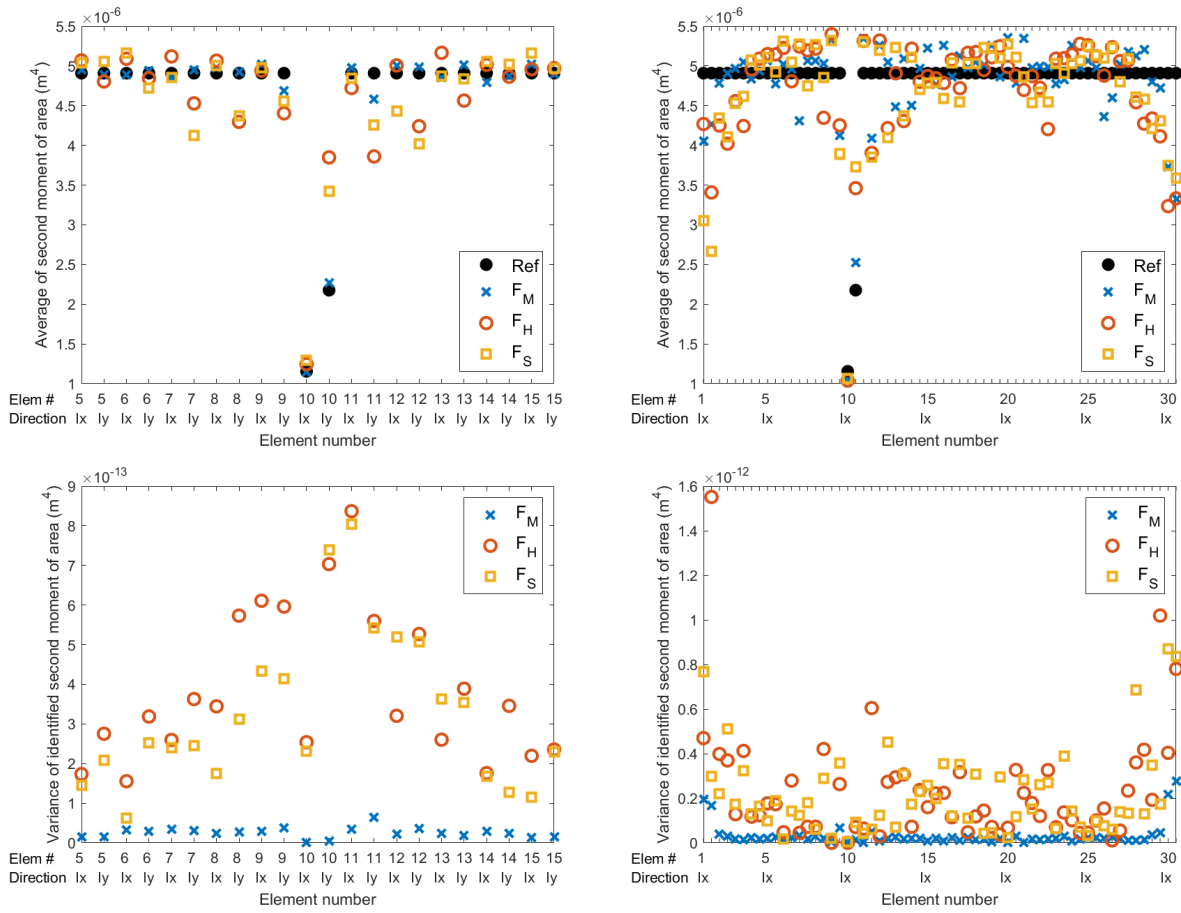
Figure 5: Top: average second moment of areas for elements 5 to 15 (left) and for elements 1 to 30 (right). Bottom: variance of the second moment of areas for elements 5 to 15 (left) and for elements 1 to 30 (right).

requires more function calls due to the narrower acceptance region than in case of $F_S(\theta)$, the evaluation of $F_M(\theta)$ does not involve data simulation, nor computation of large-size matrices, which results in a better performance.

4.2 Model optimization results

In this section a small-sample Monte Carlo study is performed for a different model parametrization sets and three objective functions. Two parameter sets are investigated:

- parameter set 1: 22 parameters corresponding to the second moments of area of elements 5 to 15 in x and y directions,

- parameter set 2: 60 parameters that correspond to the second moments of area of all the elements in x and y directions.

The population size for optimization yields 1000 and 10 realizations of the optimization algorithm are performed. The average result of the optimized parameter is depicted respectively for the first and the second parameter set in the top left and in the top right part of Figure 5. The variance of the parameter is illustrated respectively for the first and the second parameter set in the bottom left part and in the bottom right part of Figure 5.

The top part of Figure 5 illustrates that $F_M(\theta)$ yields the most accurate optimization result when compared to the other objective functions. Results obtained for the first parameter set indicate that both the damaged parameters I_x^{10} and I_y^{10}, as well as the other parameters, are well estimated when the optimization algorithm minimizes $F_M(\theta)$. The outcome of the opimization with $F_S(\theta)$ and $F_H(\theta)$ is less accurate, e.g., all the

parameters in y direction for elements between 7 and 13 are poorly estimated. The accuracy of the results obtained with $F_{\mathrm{S}}(\theta)$ and $F_{\mathrm{H}}(\theta)$ is very similar, which is expected as both objective functions are numerically identical. As for the precision of the estimates it can be clearly seen that the variance obtained from the available Monte Carlo samples is much smaller for $F_{\mathrm{M}}(\theta)$ than for $F_{\mathrm{S}}(\theta)$ and $F_{\mathrm{H}}(\theta)$. It is expected that the sample variance will decrease with the number of Monte Carlo realizations.

Results obtained for the second parameter set indicate that on average the optimization yields less accurate parameter estimates when a larger parametrization size is considered. For all three objective functions, large errors in the estimates of the second moments of area in x and y directions at the boundary elements can be observed. A possible explanation for this decrease in performance is that due to a limited number of sensors compared to the large size of FE model parametrization, the acceptance region in the respective objective functions does not only contain a single value of parameter θ, but there are many physical models that can yield the same data-driven features. As such, no separation between these models is possible, indicating that some parameter components are indistinguishable. As the goal of this work is the quantification of damage, the respective parameter changes should not be evaluated for each component individually, but should also include the dependent parameter components, as suggested in [27].

5 Conclusion

In this paper, the choice of the features for the design of the objective function to quantify structural cracks has been studied. It has been shown that the accuracy of damage identification is higher when an objective function comprising modal parameter difference is minimized, rather than for data-driven subspace-based objective functions, most likely due to the narrower acceptance region of the former. Numerical efficiency of the modal parameter-based function is also superior in terms of the computation time. All objective functions, however, are less efficient as the number of elements in the optimisation increases. In addition, identification of parameter value at the boundary conditions is subject to high variance for each objective function. Further studies using reduced order models of large finite element model will be conducted.

Acknowledgements

References

[1] A. Rytter, "Vibrational based inspection of civil engineering structures," Ph.D. dissertation, Aalborg University, Denmark, 1993, ph.D.-Thesis defended publicly at the University of Aalborg, April 20, 1993 PDF for print: 206 pp.

[2] M. Döhler, L. Mevel, and F. Hille, "Subspace-based damage detection under changes in the ambient excitation statistics," *Mechanical Systems and Signal Processing*, vol. 45, no. 1, pp. 207 – 224, 2014.

[3] M. D. Ulriksen, D. Tcherniak, P. H. Kirkegaard, and L. Damkilde, "Operational modal analysis and wavelet transformation for damage identification in wind turbine blades," *Structural Health Monitoring*, vol. 15, no. 4, pp. 381–388, 2016.

[4] K. Worden, G. Manson, and N. Fieller, "Damage detection using outlier analysis," *Journal of Sound and Vibration*, vol. 229, no. 3, pp. 647 – 667, 2000.

[5] D. Bernal, "Kalman filter damage detection in the presence of changing process and measurement noise," *Mechanical Systems and Signal Processing*, vol. 39, no. 1, pp. 361 – 371, 2013.

[6] A.-M. Yan and J.-C. Golinval, "Null subspace-based damage detection of structures using vibration measurements," *Mechanical Systems and Signal Processing*, vol. 20, no. 3, pp. 611 – 626, 2006.

[7] S. Allahdadian, M. Döhler, C. Ventura, and L. Mevel, "Towards robust statistical damage localization via model-based sensitivity clustering," *Mechanical Systems and Signal Processing*, vol. 134, p. 106341, 2019.

[8] D. Bernal and M. D. Ulriksen, "Subspace exclusion zones for damage localization," *Mechanical Systems and Signal Processing*, vol. 114, pp. 120–127, 2019.

[9] M. D. Ulriksen, D. Bernal, and L. Damkilde, "Shaped input distributions for structural damage localization," *Mechanical Systems and Signal Processing*, vol. 110, pp. 499–508, 2018.

[10] M. Ulriksen and L. Damkilde, "Structural damage localization by outlier analysis of signal-processed mode shapes – analytical and experimental validation," *Mechanical Systems and Signal Processing*, vol. 68-69, pp. 1–14, 2016.

[11] M. Döhler, L. Mevel, and Q. Zhang, "Fault Detection, Isolation and Quantification from Gaussian Residuals with Application to Structural Damage Diagnosis," *Annual Reviews in Control*, vol. 42, pp. 244–256, 2016.

[12] N. V. Hà and J.-C. Golinval, "Localization and quantification of damage in beam-like structures using sensitivities of principal component analysis results," *Mechanical Systems and Signal Processing*, vol. 24, no. 6, pp. 1831 – 1843, 2010.

[13] K. Tatsis, K. Agathos, E. Chatzi, and V. Dertimanis, "A hierarchical output-only bayesian approach for online vibration-based crack detection using parametric reduced-order models," *Mechanical Systems and Signal Processing*, vol. 167, p. 108558, 2022.

[14] K. Agathos, K. E. Tatsis, K. Vlachas, and E. Chatzi, "Parametric reduced order models for output-only vibration-based crack detection in shell structures," *Mechanical Systems and Signal Processing*, vol. 162, p. 108051, 2022.

[15] K. Agathos, K. Tatsis, S. Nicoli, S. P. Bordas, and E. Chatzi, "Crack detection in mindlin-reissner plates under dynamic loads based on fusion of data and models," *Computers & Structures*, vol. 246, p. 106475, 2021.

[16] J. Mottershead and M. Friswell, "Model updating in structural dynamics: A survey," *Journal of Sound and Vibration*, vol. 167, no. 2, pp. 347 – 375, 1993.

[17] M. Friswell and J. E. Mottershead, *Finite element model updating in structural dynamics*. Springer Science & Business Media, 2013, vol. 38.

[18] I. Behmanesh, B. Moaveni, and C. Papadimitriou, "Probabilistic damage identification of a designed 9-story building using modal data in the presence of modeling errors," *Engineering Structures*, vol. 131, pp. 542 – 552, 2017.

[19] O. Huth, G. Feltrin, J. Maeck, N. Kilic, and M. Motavalli, "Damage identification using modal data: Experiences on a prestressed concrete bridge," *Journal of Structural Engineering*, vol. 131, no. 12, pp. 1898–1910, 2005.

[20] E. Reynders, G. De Roeck, P. G. Bakir, and C. Sauvage, "Damage identification on the Tilff Bridge by vibration monitoring using optical fiber strain sensors," *Journal of Engineering Mechanics*, vol. 133, no. 2, pp. 185–193, 2007.

[21] A. Teughels and G. De Roeck, "Damage detection and parameter identification by finite element model updating," *Revue Européenne de Génie Civil*, vol. 9, no. 1-2, pp. 109–158, 2005.

[22] J.-N. Juang, *Applied system identification*. Englewood Cliffs, NJ, USA: Prentice Hall, 1994.

[23] P. van Overschee and B. de Moor, *Subspace Identification for Linear Systems*, 1st ed. Springer, 1996.

[24] E. Reynders, "System identification methods for (operational) modal analysis: Review and comparison," *Archives of Computational Methods in Engineering*, vol. 19, no. 1, pp. 51–124, Mar 2012.

[25] E. Simoen, G. De Roeck, and G. Lombaert, "Dealing with uncertainty in model updating for damage assessment: A review," *Mechanical Systems and Signal Processing*, vol. 56, pp. 123–149, 2015.

[26] S. Greś, M. Döhler, P. Andersen, and L. Mevel, "Subspace-based mahalanobis damage detection robust to changes in excitation covariance," *Structural Control and Health Monitoring*, vol. 28, no. 8, p. e2760, 2021.

[27] S. Greś, M. Döhler, and L. Mevel, "Statistical model-based optimization for damage extent quantification," *Mechanical Systems and Signal Processing*, vol. 160, p. 107894, 2021.

[28] B. Faverjon and J.-J. Sinou, "Robust damage assessment of multiple cracks based on the frequency response function and the constitutive relation error updating method," *Journal of Sound and Vibration*, vol. 312, no. 4-5, pp. 821–837, 2008.

[29] I. Mayes and W. Davies, "Analysis of the response of a multi-rotor-bearing system containing a transverse crack in a rotor," 1984.